L-band sea surface emissivity: Preliminary results of the WISE-2000 campaign and its application to salinity retrieval in the SMOS mission

A. Camps,[1] I. Corbella,[1] M. Vall-llossera,[1] N. Duffo,[1] F. Torres,[1] R. Villarino,[1] L. Enrique,[1] J. Miranda,[1] F. Julbé,[1] J. Font,[2] A. Julià,[2] C. Gabarró,[2] J. Etchetto,[3] J. Boutin,[3] A. Weill,[4] V. Caselles,[5] E. Rubio,[5] P. Wursteisen,[6] M. Berger,[6] and M. Martín-Neira[6]

Received 1 March 2002; revised 30 May 2002; accepted 4 June 2002; published 19 June 2003.

[1] Soil moisture and ocean salinity at surface level can be measured by passive microwave remote sensing at L-band. To provide global coverage data of soil moisture and ocean salinity with three-day revisit time, the Earth Explorer Opportunity Mission SMOS (Soil Moisture and Ocean Salinity) was selected by ESA (European Space Agency) in May 1999. SMOS' single payload is a Y-shaped 2-D aperture synthesis interferometric radiometer called MIRAS (Microwave Imaging Radiometer by Aperture Synthesis). SMOS presents some particular imaging peculiarities: variation of incidence and azimuth angles, different radiometric sensitivity and accuracy at each direction (pixels), and geometric polarization mixing. Therefore, the accuracy of the geophysical parameter retrieval depends on the knowledge of the angular dependence of the emissivity over a wide range of incidence and azimuth angles. The accuracy of the sea surface salinity retrievals depends on our capability to correct the wind-induced variation of the brightness temperatures. To better understand wind effects, ESA sponsored the WInd and Salinity Experiment 2000 (WISE-2000) from November 15, 2000, to January 16, 2001, in the Casablanca oil rig, at 40 km off the coast of Tarragona (Spain). This paper is divided into two parts. First, it presents the derived sensitivities of the brightness temperatures at vertical and horizontal polarizations with wind speed, and compares to Hollinger's measurements and numerical simulations. Second, these results are applied to the SMOS sea surface salinity (SSS) retrieval problem for different tracks within the swath. It is shown that, except for low SSS and sea surface temperature (SST), the retrieved SSS has a RMS error of approximately 1 psu in one satellite pass. *INDEX TERMS:* 6994 Radio Science: Instruments and techniques; 6969 Radio Science: Remote sensing; 6974 Radio Science: Signal processing; *KEYWORDS:* sea salinity, microwave radiometry, multiangular, interferometric radiometer

Citation: Camps, A., et al., L-band sea surface emissivity: Preliminary results of the WISE-2000 campaign and its application to salinity retrieval in the SMOS mission, *Radio Sci., 38*(4), 8071, doi:10.1029/2002RS002629, 2003.

1. Introduction

[2] In May 1999, the European Space Agency (ESA) selected the Earth Explorer Opportunity Mission SMOS [*Martín-Neira and Goutoule*, 1997; *Silvestrin et al*., 2001] to provide soil moisture and ocean surface salinity global coverage measurements with three-day revisit time. SMOS' payload is MIRAS that will be the first two-dimensional synthetic aperture radiometer for Earth observation. Its scanning configuration presents new challenges, mainly two-dimensional imaging of the scene, with varying pixel resolution, azimuth and inci-

[1]Department of Signal Theory and Communications, Universitat Politècnica de Catalunya, Barcelona, Spain.
[2]Institut de Ciències del Mar, CMIMA-CSIC, Barcelona, Spain.
[3]LODYC, Université Pierre et Marie Curie, Case 100, Paris, France.
[4]Centre d'étude des Environnements Terrestre et Planétaires, Vélizy, France.
[5]Deparment of Thermodynamics, Faculty of Physics, Valencia, Spain.
[6]European Space Agency, European Space Research and Technology Centre, Noordwijk, Netherlands.

0048-6604/03/2002RS002629$11.00

dence angles as the pixel travels through the alias-free field of view.

[3] Sea surface salinity can be measured by passive microwave remote sensing at L-band, where there is a reserved frequency band (1.400-1.427 MHz). This frequency band is a compromise between the sensitivity of the brightness temperature to the salinity, small atmospheric perturbation and reasonable pixel resolution [*Swift and McIntosh*, 1983]. The WISE 2000 campaign was sponsored by ESA to collect experimental data under the widest possible range of wind conditions to better understand the polarimetric emission at L-band of the sea surface and its dependence with wind and salinity. The WISE-2000 campaign took place at the Casablanca oil rig, located at 40° 43' 4″ N 1° 21' 34″ E, 40 km away from the Ebro river mouth, at the coast of Tarragona (Spain), where sea conditions are representative of the open Mediterranean with periodic influence of the Ebro river fresh water plume. Systematic measurements were acquired from November 16th to December 18th, 2000 and continued during January 9th to 15th, 2001.

[4] The WISE 2000 participants were the Polytechnic University of Catalonia (UPC, Barcelona, Spain, prime contractor), the Institut of Marine Sciences (ICM-CSIC, Barcelona, Spain), the Laboratoire d'Océanographie Dynamique et Climatologie (LODYC, Paris, France), the University of València (UV, València, Spain), the Centre d'Études Terrestres et Planétaires (CETP, Paris, France) and the University of Massachusetts–Amherst (UMass, USA) as a guest institution.

[5] The following instruments were deployed: (1) an L-band polarimetric radiometer (UPC), (2) a Ka-band polarimetric radiometer (UMass), (3) a stereo-camera to determine topography and RMS slopes of the sea surface (CETP), (4) three oceanographic and climatological buoys with salinity, temperature, wind speed and direction, wave height and period sensors etc. (ICM-CSIC and LODYC), (5) a portable meteorological station (UPC) with atmospheric pressure, air temperature, relative humidity and rain rate sensors, (6) a video camera (UPC) mounted on the L-band radiometer pedestal to determine sea surface foam coverage, and (7) an IR radiometer (UV) to determine sea surface temperature estimates. In addition, simultaneous satellite imagery was acquired: AVHRR-derived sea surface temperature, SeaWifs ocean color, and QuickScat wind speed. (Quickscat data were acquired in neighbor pixels to the south and east, free from coastal effects.)

2. Results of the WISE-2000 Campaign

[6] The analysis of the data acquired by the different sensors is described in detail by *Camps et al*. [2002].

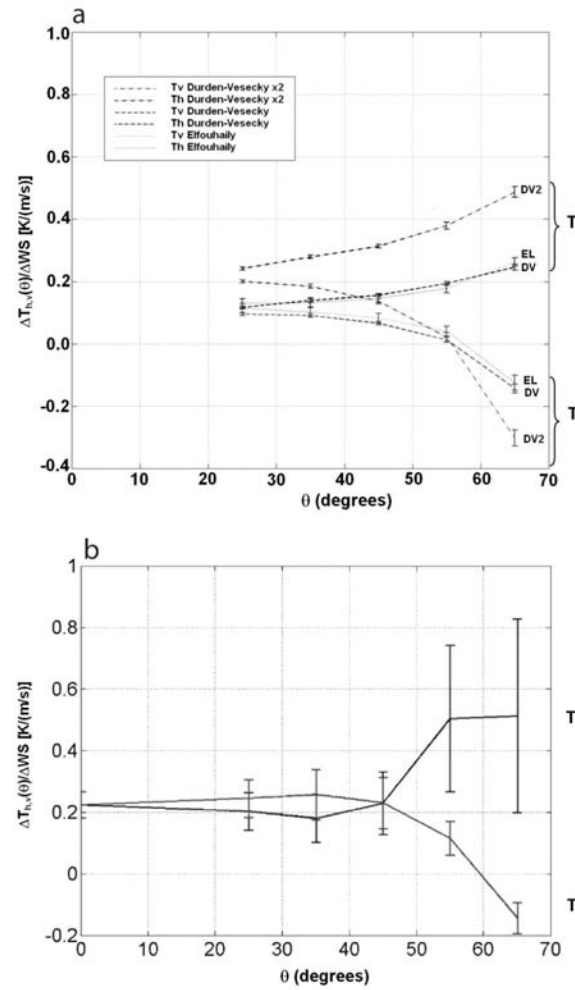

Figure 1. (a) WISE 2000-derived brightness temperature sensitivities to wind speed versus incidence angle at vertical and horizontal polarizations: 1-σ error bars computed from radiometric error and wind speed measurement error. Larger error bars at horizontal polarization and large incidence angles due to lower number of available data points (eliminated because corrupted by RFI). (b) Simulated brightness temperature sensitivities under WISE conditions using the *Yueh* [1997] two-scale model and the *Elfouhaily et al.* [1997] and *Durden and Vesecky* [1985] sea surface spectrum, multiplied by 1 and 2.

Figure 1 shows the derived sensitivity of the horizontal and vertical brightness temperatures to wind speed (circles), derived by fitting the radiometric data obtained over the whole range of wind speeds (WS = 0–18 m/s) with least squares regression lines. When compared with the ones derived from *Hollinger*'s [1971] measurements (diamonds) and the numerical simulations performed with a two-scale model [*Yueh*, 1997] using the *Durden and Vesecky* [1985] sea spectrum multiplied by two and

run in the observed WISE SSS, SST and WS conditions (solid line) (E. Dinnat, personal communication), experimental results show a nadir sensitivity of 0.22 K/(m/s), increasing with incidence angle at horizontal polarization, and decreasing at vertical polarization, being null between 55° and 60°.

[7] Figure 2 shows the measured azimuthal variation (circles) of the first three Stokes parameters at constant incidence angles and model results obtained using a modification of the *Camps and Reising* [2001] model at low frequency. The largest azimuthal variation of the first two Stokes parameters is on the order of 0.1–0.2 K approximately, much smaller than the noise level in any SMOS pixel (≈ 5 K), and therefore will be ignored in the salinity retrieval process (section 3). (These results have to be confirmed by the results of the ongoing ESA-sponsored LOSAC campaign.)

[8] The SSS retrieval requires the knowledge of WS and SST ancillary data. Most often, wind stress and sea state was correlated and WS and direction can be used to describe its state. Even though it was found a good agreement between buoy data, meteorological station data and Quickscat imagery, the intercomparison of different WS measurements showed an associated RMS error ~1.7–2.5 m/s [*Camps et al*., 2002], and taking these WS inputs as fixed parameters, the induced error in the retrieved SSS may be very important. In other situations, the correlation between wind stress and sea state was quite low. A characterization and modeling of the swell would be required, which will be the object of future studies.

[9] SST estimates from the IR radiometer and AVHRR imagery have proven to be accurate enough for the SSS retrieval process, exhibiting a small bias (~-0.2 K) that increases at high wind speeds, probably because of a lack of accurate models of the sea foam emissivity at the IR.

3. Sea Surface Salinity Retrieval in the SMOS Configuration

[10] SSS has already been retrieved from L-band radiometric measurements at constant incidence angles [*Miller et al.*, 1998]. However, the SMOS configuration presents a particularity: the same pixel is observed under different views at different incidence angles, with varying spatial resolution, radiometric accuracy and sensitivities, depending on the position of each pixel with respect to the cross-track. Figure 3 represents this particular imaging characteristic for the selected SMOS configuration. The arrows indicate the tracks followed by a pixel, since it enters in the field of view (top), until it leaves it (bottom). Depending on the distance with respect to the satellite ground track, the number of snapshots in which the pixel will be imaged will vary. As it goes far away

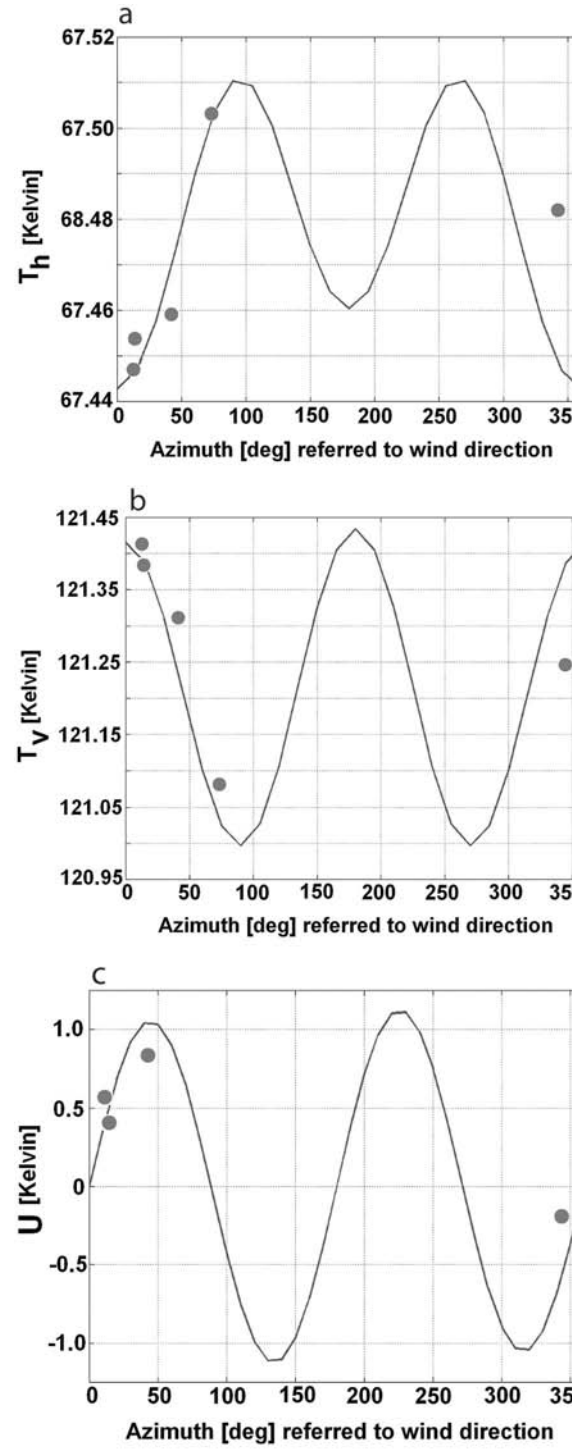

Figure 2. (a) T_h, (b) T_v and (c) U azimuth scans at θ = 45°, WS = 2.8 m/s, SST = 14.1°C, SSS = 37.9 psu (data: circles, model fit: solid line). See color version of this figure at the back of this issue.

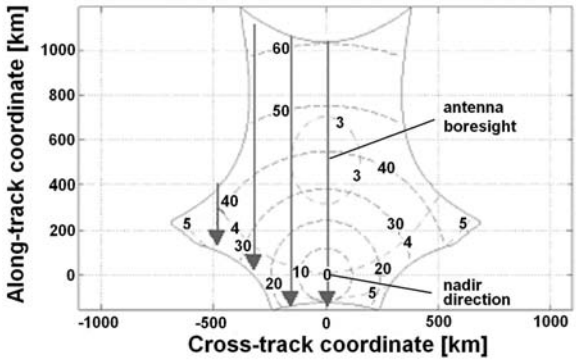

Figure 3. The SMOS imaging characteristics: a pixel is imaged many times under different incidence angles (0°-60°), with different spatial resolutions and radiometric sensitivities (>3K). Parameters: 21 antennas per arm, d = 0.875 wavelengths antenna spacing, $\beta = 32°$ tilt angle, and h = 755 km platform height.

from the ground track, not only it is imaged less and less times, but also the angular variation is reduced and measurements become noisier, which translates in a degraded performance in terms of the retrieved parameters.

[11] The SSS retrieval problem presents some difficulties that are listed below:

1. The first is the effect of wind. At nadir, the sensitivity of the brightness temperatures to SSS is $\Delta T_{v,h}(\theta)/\Delta SSS \approx 0.5$ K/psu at SST=25°C (Figure 4a)), and that to WS is $\Delta T_{v,h}(\theta)/\Delta WS \approx 0.2$ K/(m/s) (Figure 1a). Taking into account the range of variability of the SSS (30-38 psu) and the WS (0 to ~25m/s), WS masks the SSS signature, unless it is properly corrected.

Since the wind produces a small variation on the brightness temperatures at both polarizations ($T_{h,v}$), a first order approximation has been used to model its effect:

$$T_{h,v}(\theta,SST,SSS,WS) \approx e_{h,v}^{Fresnel}(\theta,SST,SSS)\cdot SST + \frac{\Delta T_{h,v}(\theta)}{\Delta WS}\cdot WS \quad (1)$$

where $\Delta T_{v,h}(\theta)/\Delta WS$ is the sensitivity of the brightness temperatures to wind speed (Figure 1) and $e_{h,v}^{Fresnel}$ is the emissivity of a perfectly flat sea surface (no wind), which is related to the electric field Fresnel reflection coefficients $\Gamma_{v,h}$ by

$$e_{v,h}^{Fresnel}(\theta,STT,SSS) \triangleq 1 - |\Gamma_{v,h}(\Delta,SST,SSS)|^2. \quad (2)$$

2. The second difficulty presented by the SSS retrieval problem is polarization mixing. SMOS images a very wide two-dimensional field of view, tailored to provide three-day revisit time at the equator. However,

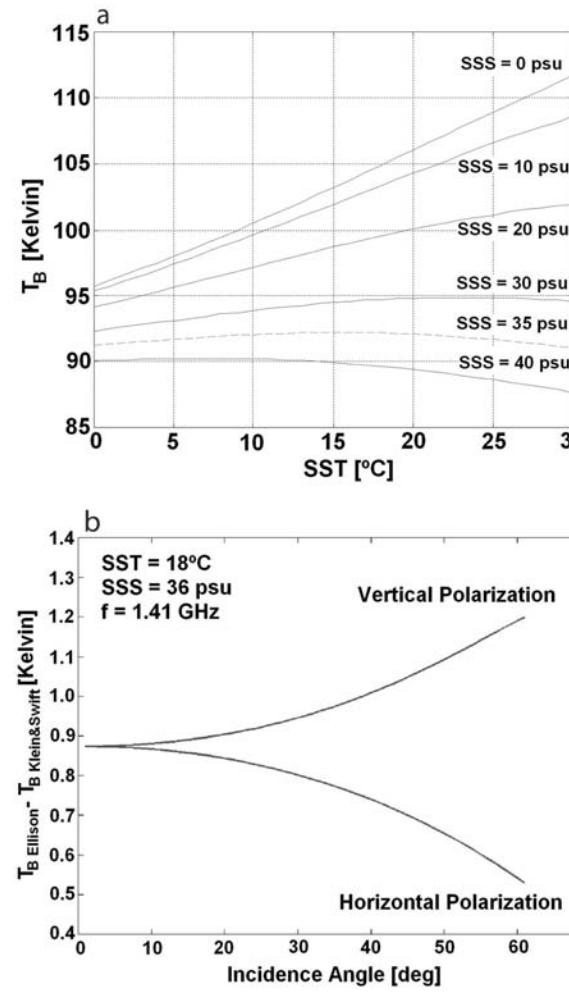

Figure 4. (a) Dependence of the brightness temperature at nadir with SSS and SST. (b) Incidence angle dependence of the difference between brightness temperatures computed using *Ellison et al*. [1998] or *Klein and Swift* [1977] seawater permittivity model (SST = 18°C, SSS = 36 psu, F = 1.41 GHz). See color version of this figure at the back of this issue.

as we move away from the E- and H- planes of the antennas, there is a polarization mixing between vertical and horizontal polarizations [*Claasen and Fung*, 1974]. That is, the brightness temperatures in the antenna reference frame are related to the brightness temperatures in the local reference frame over the Earth by

$$\begin{bmatrix} T_V \\ T_H \end{bmatrix}^{(ant)} = \begin{bmatrix} \cos^2\psi & \sin^2\psi \\ \sin^2\psi & \cos^2\psi \end{bmatrix} \begin{bmatrix} T_V \\ T_H \end{bmatrix}^{(pixel)}, \quad (3)$$

where the angle ψ depends on the observation geometry. The angle ψ also depends on the Faraday rotation that cannot be neglected at L-band. (Estimates to be used in

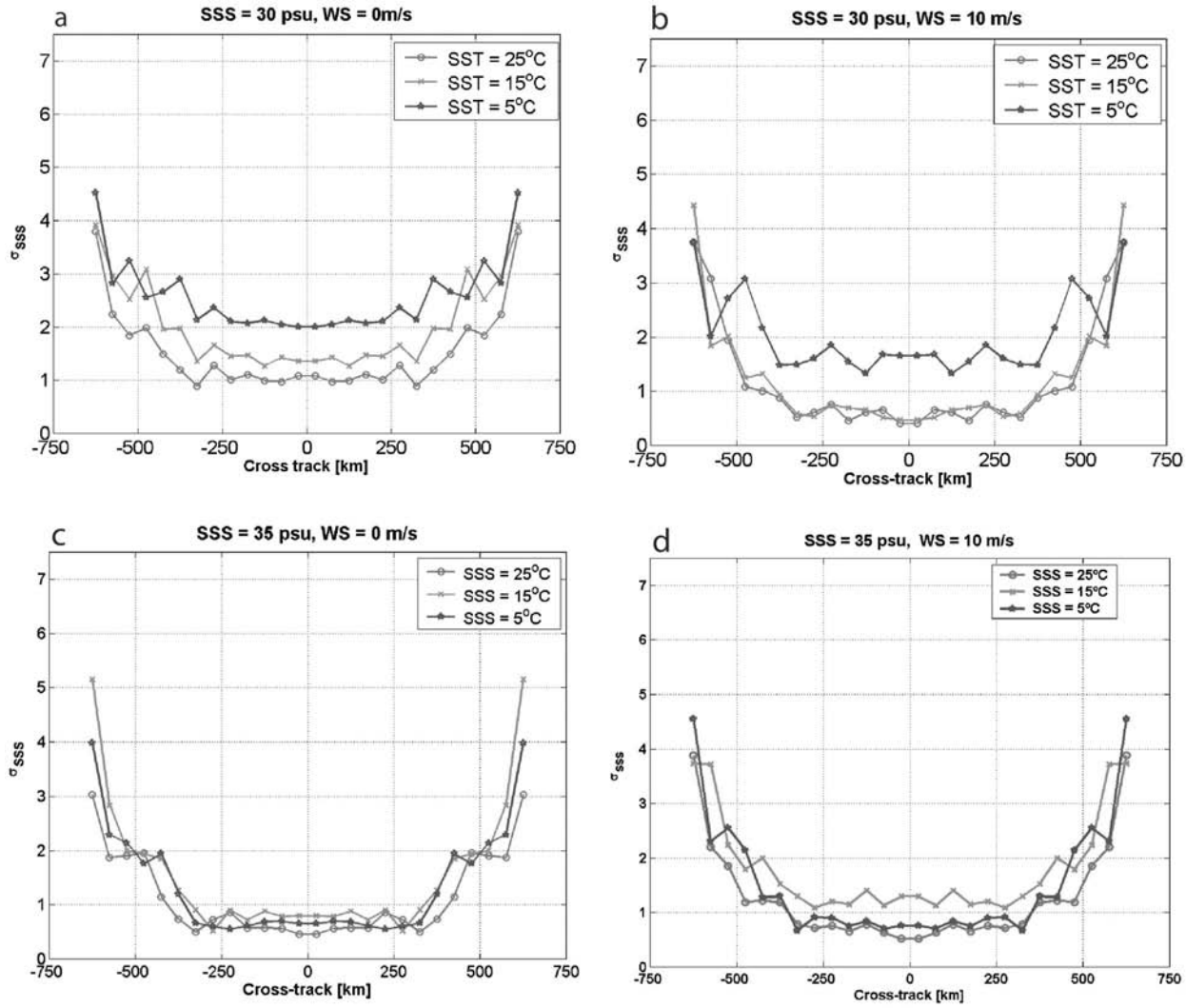

Figure 5. Simulated standard deviation of the retrieved SSS for different wind speed 0 m/s (left) and 10 m/s (right), different SSS (a and b) 30 psu, (c and d) 35 psu and (e and f) 40 psu, and different SST: 5°C (stars), 15°C (crosses) and 25°C (circles). See color version of this figure at the back of this issue.

equation (3) may be used, but their accuracy is not good enough for the required SSS accuracy. Additionally, local ionospheric inhomogeneities create different Faraday rotations within a pixel.)

[12] The polarization mixing problems (geometry plus Faraday rotation) can be avoided if the retrieval problem is formulated in terms of the first Stokes parameter I defined as

$$I = T_v^{ant} + T_H^{ant} = T_V^{pixel} + T_H^{pixel}, \tag{4}$$

which is invariant to rotations, as it can be readily deduced from equation (3). A second advantage of this approach is that it minimizes the effect of the uncertainty in the dielectric permittivity models (*Klein and Swift* [1977] or *Ellison et al.* [1998]). Since the sum of the two plots in Figure 4b is approximately constant, this uncertainty appears as an offset. Additionally, the sensitivity of I to SST is ~0.6 K/(m/s), smaller reduced from that if T_V were used.

[13] The proposed SSS retrieval algorithm is based on the minimization of the error defined as

$$\varepsilon = \frac{1}{N_{observations}} \sum_n \left[(I^{model}(\theta_n, S\hat{S}S, S\hat{S}T, \hat{W}S) - I^{data}(\theta_n, SSS, SST, WS)) \frac{t(\theta,\phi)}{\cos\theta} \right]^2, \tag{5}$$

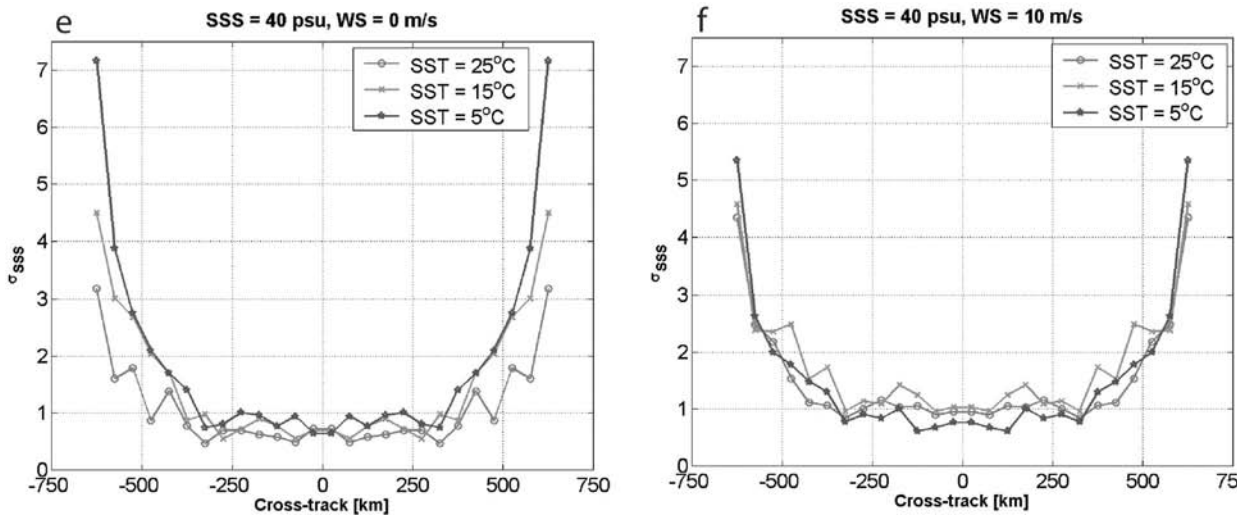

Fig 5. Continued.

where $N_{observations}$ is the total number of measurements in a given pixel track (Figure 3) only limited by the alias-free FOV, I^{model} is the first Stokes parameter ($I^{model}(\hat{SSS},\hat{SST},\hat{WS}) = T_V^{ant} + T_H^{ant}$) computed from the model with the estimated $\hat{SSS}$,$\hat{SST}$, and $\hat{WS}$ parameters (azimuthal dependence is negligible and therefore is not included in the modeling), I^{data} corresponds to the first Stokes parameter evaluated from the sum of consecutive T_h and T_v measurements in a pixel by pixel basis (each one observed under a different incidence angle θ_n) and $t(\Delta,\phi)/\cos\theta$ is the normalized antenna radiation pattern divided by the obliquity factor used to give more weight to the samples with the better radiometric sensitivity.

[14] In this study, I^{data} contains simulated data computed from equations (1) and (2) and a pixel-dependent random noise error that depends on the angular distance to the boresight. Therefore, simulations show the best results that could be achieved in one satellite passage with an ideal error-free instrument. The minimization problem uses the Levenberg-Marquardt method available in the Matlab© optimization toolbox, with restrictions for SSS (30-40 psu), SST (0-40°C), and WS (0-30 m/s). Since the sensitivity to SSS of the function being minimized is low (equation (5)), the speed and accuracy of the retrieval is improved by reducing the search limits to an interval centered around the values that could be provided by other sensors and an interval length given by their associated error bounds ($\hat{SST} \in [SST_0 - 1°C, SST_0 + 1°C]$ and $\hat{WS} \in [WS_0 - 2.5$ m/s, $WS_0 + 2.5$ m/s]). It is found that this approach produces better results than forcing the measured SST_0 and WS_0 values, which may have an error with respect to the real values SST and WS used to generate the "simulated" data (equation (5)).

[15] Figure 5 shows the standard deviation of the retrieved $\hat{SSS}(\sigma_{\hat{SSS}-SSS})$ for different wind speeds 0 m/s (left) and 10 m/s (right), different SSS (Figures 5a and 5b) 30 psu (Figures 5c and 5d), 35 psu and (Figures 5e and 5f) 40 psu, and different SST: 5°C (stars), 15°C (crosses) and 25°C (circles).

[16] The following is observed:

1. In general, SSS retrieval improves with increasing SST, except for high SSS and WS. The reason for that is not know, but it is suspected that its due to the change in the slope of T_B(SST) from 35 psu to 40 psu.

2. As expected, because of the lower number of samples and the higher noise, SSS estimates worsen at swath edges because of higher noise level.

3. Forcing the values of $\hat{SST} = SST_0$ and $\hat{WS} = WS_0$ to the "measured" values (including the measurement errors: ±1°C, ±2.5 m/s) induces a larger error in $\hat{SSS}$, than letting them be adjusted by the minimization algorithm.

4. As shown in Figure 6, the $\hat{SSS}$ error includes a bias (positive or negative), and a random error. In general, at low WS, the estimated $\hat{WS}$ tends to be higher (positive bias), which the algorithm compensates increasing the estimated $\hat{SSS}$ (positive bias). At higher WS, the situation is reversed. In all cases, the adjusted $\hat{SST}$ has a negligible bias.

5. The retrieved $\hat{SSS}$ has an error of approximately ≈1 psu, in one satellite passage, in a swath of ± 300 km from the satellite ground track.

4. Conclusions

[17] Brightness temperatures sensitivities to wind speed derived from WISE-2000 data confirm existing experimental data [*Hollinger*, 1971] and are in agree-

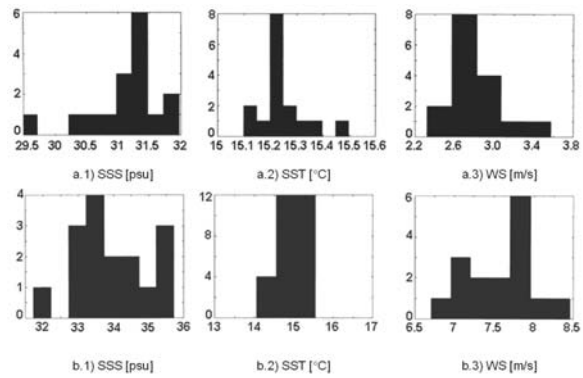

Figure 6. Typical histograms of retrieved $\hat{SSS}$, $\hat{SST}$ and $\hat{WS}$ for (a) SSS = 30 psu, SST = 15°C and WS = 0 m/s (positive bias in SSS and WS); (b) SSS = 35 psu, SST = 15°C and WS = 10 m/s (negative bias in SSS and WS), computed from 16 simulation with different random noise.

ment with numerical results predicted by a two-scale model using *Durden and Vesecky* [1985] sea spectrum multiplied by two. At 25° incidence angle, the experimental results show a sensitivity of 0.24 K/(m/s) and 0.20 K/(m/s) at vertical and horizontal polarization. At higher incidence angles, the sensitivity to wind speed increases at horizontal polarization, and decreases at vertical polarization, being null between 55° and 60° incidence angle. The maximum azimuthal variation is very small ($\Delta T_{h,v\ \text{peak-to-peak}} \sim 0.1–0.2$ K). More data needs to be acquired to improve the determination of the sensitivities to wind speed, mainly at large incidence angles, and foam and swell effects need to be accounted for to improve the emissivity models.

[18] These results have been applied to a performance study of an SMOS-oriented SSS retrieval algorithm. To avoid geometrical and Faraday-rotation polarization mixing, the algorithm is based in the minimization of the error between the sum of the measured T_h and T_v and the sum of the modeled T_h and T_v, for different pixel tracks in the alias-free FOV. Except for low SSS and low SST, the retrieved SSS have an error of approximately 1 psu, within a $\pm$300 km swath, in one satellite passage. Since part of this error is a bias, further research will be focused on its reduction in several satellite passages in a 10 to 30 day interval, wind conditions will be different, and the study of instrumental systematic errors.

[19] **Acknowledgments.** The WISE 2000 campaign has been sponsored by the European Space Agency under ESTEC contract 14188/00/NL/DC. The sea emission numerical simulations have been performed under ESTEC Salinity Study 3618. We thank the Centre National d'Études Spatiales for the French moorings and Météo France for help in the buoy data handling. The implementation of the L-band AUtomatic RAdiometer (LAURA) of the Polytechnic University of Catalonia and the SSS retrieval study have been supported by the Spanish government under grant CICYT TIC 99-1050-C03-01. The friendly cooperation and help provided by the personnel of Repsol Investigaciones Petrolíferas–Base Tarragona–Plataforma Casablanca for the organization of the campaign is greatly appreciated.

References

Camps, A., and S. C. Reising, A model for the wind direction signature in the Stokes emission vector of the ocean surface at microwave frequencies, *Microwave Opt. Technol. Lett.*, *29*(6), 426–432, 2001.

Camps, A., et al., Sea surface emissivity observations at L-band: First results of the Wind and Salinity Experiment WISE-2000, *IEEE Trans. Geosci. Remote Sens.*, *40*(10), 2117–2130, 2002.

Claasen, J. P., and A. K. Fung, The recovery of polarized apparent temperature distributions of flat scenes from antenna temperature measurements, *IEEE Trans. Antennas Propag.*, *22*(3), 433–442, 1974.

Durden, S. L., and J. F. Vesecky, A physical radar cross-section model for a wind-driven sea with swell, *IEEE J. Oceanic Eng.*, *10*(4), 445–451, 1985.

Elfouhaily, T., B. Chapron, K. Katsaros, and D. Vandemark, A unified directional spectrum for long and short wind-driven waves, *J. Geophys. Res.*, *102*, 15,781–15,796, 1997.

Ellison, W., A. Balana, G. Delbos, K. Lamkaouchi, L. Eymard, C. Guillou, and C. Prigent, New permittivity measurements of sea water, *Radio Sci.*, *33*(3), 639–648, 1998.

Hollinger, J. P., Passive microwave measurements of sea surface roughness, *IEEE Trans. Geosci. Electron.*, *9*(3), 165–169, 1971.

Klein, L. A., and C. T. Swift, An improved model for the dielectric constant of sea water at microwave frequencies, *IEEE J. Oceanic Eng.*, *2*(1), 104–111, 1977.

Martín-Neira, M., and J. M. Goutoule, A two-dimensional aperture-synthesis radiometer for soil moisture and ocean salinity observations, *ESA Bull.*, *92*, 95–104, 1997.

Miller, J. L., M. A. Goodberlet, and J. B. Zaitzeff, Airborne salinity mapper makes debut in coastal zone, *Eos Trans. AGU*, *79*(14), 173–177, 1998.

Silvestrin, P., M. Berger, Y. Kerr, and J. Font, ESA's second Earth Explorer Opportunity Mission: The Soil Moisture and Ocean Salinity mission–SMOS, *IEEE Geosci. Remote Sens. Newsl., Cumul. Issue 118*, 11–14, 2001.

Swift, C. T., and R. E. McIntosh, Considerations for microwave remote sensing of ocean surface salinity, *IEEE Trans. Geosci. Remote Sens.*, *21*(4), 480–491, 1983.

Yueh, S. H., Modeling of wind direction signals in polarimetric sea surface brightness temperatures, *IEEE Trans. Geosci. Remote Sens.*, *35*(6), 1400–1418, 1997.

M. Berger, M. Martín-Neira, and P. Wursteisen, European Space Agency, European Space Research and Technology Centre, Keplerlaan 1, 2200-AG Noordwijk, Netherlands.

J. Boutin and J. Etchetto, LODYC, UPMC, Case 100, Tour 15 2e étage, 4 Pl Jussieu, 75252 Paris Cedex 05, France.

A. Camps, I. Corbella, N. Duffo, L. Enrique, F. Julbé, J. Miranda, F. Torres, M. Vall-llossera, and R. Villarino, Department of Signal Theory and Communications, Universitat Politècnica de Catalunya, Campus Nord-D3, Jordi Girona 1-3, 08034 Barcelona, Spain. (camps@tsc.upc.es)

V. Caselles and E. Rubio, Department of Thermodynamics, Faculty of Physics, Dr. Moliner 50, 46100 Burjassot, Valencia, Spain.

J. Font, C. Gabarró, and A. Julià, Institut de Ciències del Mar, CMIMA-CSIC, Passeig Marítim 37-49, 08003 Barcelona, Spain.

A. Weill, CETP, 10-12 av de l'Europe, 78140 Vélizy, France.